

Classification of Coupled-Channel Near-Threshold Structures

Zhen-Hua Zhang^{1,2,*} and Feng-Kun Guo^{1,2,3,4,†}

¹*CAS Key Laboratory of Theoretical Physics, Institute of Theoretical Physics,
Chinese Academy of Sciences, Beijing 100190, China*

²*School of Physical Sciences, University of Chinese Academy of Sciences, Beijing 100049, China*

³*Peng Huanwu Collaborative Center for Research and Education, Beihang University, Beijing 100191, China*

⁴*Southern Center for Nuclear-Science Theory (SCNT), Institute of Modern Physics,
Chinese Academy of Sciences, Huizhou 516000, China*

Since 2003, plenty of resonant structures have been observed in the heavy quarkonium regime. Many of them are close to the thresholds of a few pairs of heavy hadrons. They are candidates of exotic hadrons and have attracted immense attentions. Based on a coupled-channel nonrelativistic effective field theory, we classify the near-threshold structures of a symmetry-related two-channel system according to the scattering length and channel coupling strength. We show that the evolution of the scattering amplitude line shapes can be understood from the pole trajectories in the complex energy plane, and the pole evolution can be traced back to the renormalization group fixed points. We provide a dictionary of correspondence between the evolution of line shapes and pole trajectories, which can be used to understand the experimental observations of the near-threshold structures.

I. INTRODUCTION

In the past two decades, plethora of resonant structures have been observed in the invariant mass distribution of heavy hadrons at the high energy experiment, and have attracted lots of attentions and debates. Strenuous efforts have been made to understand how these resonances emerge from underlying strong interactions and what internal structures they have, while consensus on these questions has not been achieved (for reviews, see Refs. [1–9]).

A surprising and prominent feature is that many of the resonant structures are close to the threshold of a pair of hadrons containing heavy quarks, *e.g.*, the famous $X(3872)$ is located in the immediate vicinity of the $D^0\bar{D}^{*0}$ threshold [10–12]. A general explanation about these near-threshold structures has been given in Ref. [13], which shows that a nontrivial peak or dip structure close to the threshold of a pair of heavy hadrons must appear if they have S -wave attractive interaction. However, such construction still needs to be generalized to situations where the resonant structures are close to more than one threshold, which is often the physical situation and the line shapes can be more complicated because of the intertwined energy dependence of the amplitude caused by multiple thresholds. For instance, among recent experimental discoveries, while the $X(3872)$ mass coincides with the $D^0\bar{D}^{*0}$ threshold within uncertainties [14], the D^+D^{*-} threshold is only about 8 MeV away; the $X(6900)$ in the double J/ψ spectrum [15–17] is close to the $J/\psi\psi(2S)$ and $J/\psi\psi(3770)$ thresholds [18]; the $T_{c\bar{s}}(2900)$ seen in the $D_s^+\pi^-$ and $D_s^+\pi^+$ invariant mass distributions in the $B^0 \rightarrow \bar{D}^0 D_s^+ \pi^-$ and $B^+ \rightarrow D^- D_s^+ \pi^+$ decays [19, 20] is close to the $D_s^* \rho$ and

D^*K^* thresholds [21]; the $T_{cc}^+(3875)$ in the $D^0 D^0 \pi^+$ invariant mass distribution [22, 23] is just below the $D^{*+} D^0$ and $D^{*0} D^+$ thresholds [24–26]; the $P_{cs}(4338)^0$ observed in the $J/\psi\Lambda$ spectrum [27] is very close to the $\Xi_c^0 \bar{D}^0$ and $\Xi_c^+ D^-$ thresholds [28]; and the $X(3960)$ in the $D_s^+ D_s^-$ spectrum [29, 30] is close to the $D_s^+ D_s^-$ and $D^* \bar{D}^*$ thresholds [31]; and so on. These are just some representatives of the structures close to at least two nearby thresholds, and most of the nearby channels are related by some kind of symmetry, *e.g.*, isospin symmetry, SU(3) symmetry, and/or heavy quark spin symmetry. The resonance line shapes are intricately distorted by these thresholds, and a classification of the general behavior near multiple thresholds is called for.

In this Letter, we classify the general line shape behavior near multiple thresholds with evolutions of the scattering length and channel coupling strength, starting from the renormalization group (RG) fixed points (FPs) in the framework of a coupled-channel zero-range effective field theory (ZREFT). For simplicity, we will discuss a system with two symmetry-related nearby channels and the discussion can be generalized to systems with more channels.

II. RENORMALIZATION GROUP FIXED POINTS

We consider a two-channel system (channel-1 and channel-2) with nearby thresholds denoted as Σ_1 and Σ_2 , with $\Delta \equiv \Sigma_2 - \Sigma_1 > 0$. The corresponding reduced masses are represented by M_1 and M_2 , respectively. We will focus on the line shapes near the two thresholds, and therefore both channels will be treated nonrelativistically. We define the center-of-mass (c.m.) energy relative to the first threshold as $E = \sqrt{s} - \Sigma_1$, with \sqrt{s} being the total c.m. energy.

We first review the RG treatment to the two-channel scattering derived in Ref. [32]. For the on-shell S -wave

* zhangzhenhua@itp.ac.cn

† Corresponding author, fkguo@itp.ac.cn

scattering processes, the scattering potential only depends on the c.m. energy [32] (*i.e.*, separable potential), and thus the Lippmann-Schwinger equation (LSE) for the two-channel scattering amplitude can be written as an algebraic equation

$$\mathbf{T}(p_1, \delta_1) = \mathbf{V}(p_1, \delta_1) + \mathbf{V}(p_1, \delta_1)\mathbf{J}(p_1, \delta_1)\mathbf{T}(p_1, \delta_1), \quad (1)$$

where $p_1 = \sqrt{2M_1E}$ and $\delta_1 = \sqrt{2M_1\Delta}$ are small momentum scales, the ultraviolet divergent Green's function $\mathbf{J}(p_1, \delta_1)$ can be regularized by the dimensional regularization with the power divergence subtraction scheme [33, 34] as

$$\mathbf{J}(p_1, \delta_1, \mu) = -\frac{1}{2\pi}\mathbf{M}^{1/2}(\mu\mathbf{I}_{2\times 2} + i\mathbf{P})\mathbf{M}^{1/2}, \quad (2)$$

where μ is the subtraction scale, $\mathbf{P} = \text{diag}(p_1, p_2)$ with p_1 and $p_2 = \sqrt{2M_2(E - \Delta)}$ the magnitudes of the c.m. momenta of particles in channel-1 and channel-2, respectively, and $\mathbf{M} = \text{diag}(M_1, M_2)$.

The scale independence of the scattering amplitude gives the RG equation (RGE) of the potential $\mathbf{V}(p_1, \delta_1, \mu)$,

$$\mu \frac{\partial \hat{\mathbf{V}}}{\partial \mu} = \hat{p} \frac{\partial \hat{\mathbf{V}}}{\partial \hat{p}} + \hat{\delta} \frac{\partial \hat{\mathbf{V}}}{\partial \hat{\delta}} + \hat{\mathbf{V}} + \hat{\mathbf{V}}^2, \quad (3)$$

where $\hat{p} \equiv p_1/\mu$, $\hat{\delta} \equiv \delta_1/\mu$, and $\hat{\mathbf{V}} = \mu/(2\pi)\mathbf{M}^{1/2}\mathbf{V}\mathbf{M}^{1/2}$. Its scale invariant solutions are the RG FPs. There are three types of FPs for a two-channel system [32]: the trivial FP corresponding to vanishing interaction:

$$\hat{\mathbf{V}}_0 = 0, \quad (4)$$

the FP with two bound/virtual states at the threshold:

$$\hat{\mathbf{V}}_2 = -\mathbf{I}_{2\times 2}, \quad (5)$$

and the FP with only one bound/virtual state at the threshold:

$$\hat{\mathbf{V}}_1 = \begin{pmatrix} -c & \pm\sqrt{c(1-c)} \\ \pm\sqrt{c(1-c)} & -(1-c) \end{pmatrix}. \quad (6)$$

The general scattering amplitude can be derived from the LSE using the potential solved from the RGE near the RG FPs. Keeping only constant contact terms in the potential, the scattering amplitude reads [32]

$$\mathbf{T} = 2\pi\mathbf{M}^{-1/2}\mathbf{R} \begin{pmatrix} -\frac{1}{a_{11}} + ip_{11} & \frac{1}{a_{12}} + ip_{12} \\ \frac{1}{a_{12}} + ip_{12} & -\frac{1}{a_{22}} + ip_{22} \end{pmatrix}^{-1} \mathbf{R}^T\mathbf{M}^{-1/2}, \quad (7)$$

with

$$\mathbf{R} = \begin{pmatrix} \cos \phi & -\sin \phi \\ \sin \phi & \cos \phi \end{pmatrix} \in \text{SO}(2), \quad (8)$$

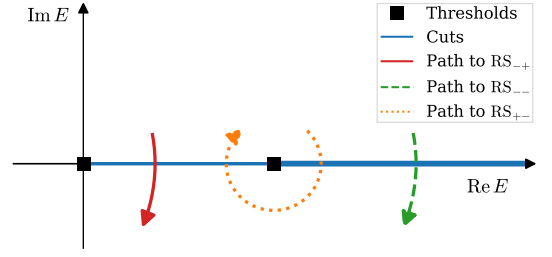


FIG. 1. The shortest paths from the physical region to different unphysical RSs.

and $p_{ij} = (\mathbf{R}^T\mathbf{P}\mathbf{R})_{ij}$. Parameters a_{11} and a_{22} are the single-channel scattering lengths. The channel coupling is provided by a finite $|a_{12}|$ and induces an effective attraction in channel-1 and repulsion in channel-2 (see, *e.g.*, Refs. [21, 35]). Near different FPs, the scattering lengths have different scalings and thus lead to different power countings for the scattering amplitude [32]. The amplitude near the trivial FP $\hat{\mathbf{V}}_0 = 0$ describes a weakly interacting system and is not of interest here.

Near the FP $\hat{\mathbf{V}}_1$ in Eq. (6), which can be rewritten using the rotation in Eq. (8) as $\hat{\mathbf{V}}_1 = -\mathbf{u}\mathbf{u}^T$ with $\mathbf{u} = (\cos \phi, \sin \phi)^T$ [32], one can take $|a_{11}^{-1}| < \mu$, $|a_{22}^{-1}| \gg \mu$, and the leading order (LO) amplitude reads

$$\mathbf{T}^{\text{LO}} = \frac{2\pi}{-a_{11}^{-1} + ip_{11}}\mathbf{M}^{-1/2}\mathbf{R} \begin{pmatrix} 1 & 0 \\ 0 & 0 \end{pmatrix} \mathbf{R}^T\mathbf{M}^{-1/2}, \quad (9)$$

which describes a system with one near-threshold bound/virtual state.

Near the FP $\hat{\mathbf{V}}_2$ in Eq. (5), one has $|a_{11}^{-1}| < \mu$, $|a_{22}^{-1}| < \mu$. The LO scattering amplitude near this FP has the same form as Eq. (7), and describes a system with two bound/virtual states near the thresholds [36].

III. LINE SHAPES AND POLES

With these LO scattering amplitudes, one can classify the LO near-threshold behaviors of the scattering amplitude line shapes according to the pole locations evolved from the RG FPs. As is well-known (see, *e.g.*, Refs. [3, 6, 13]), if the pole is located on a Riemann sheet (RS) that can reach the physical region only by going around a threshold, its effects will manifest as a cusp, exactly at threshold. The width of the cusp depends on the distance of the pole to the physics region. For simplicity, we consider symmetry related channels by imposing $a_{22} = a_{11}$ in Eq. (7). Without loss of generality, we will show pole trajectories and line shapes with the masses of the particles in the two channels being those of $D^0\bar{D}^{*0}$ and D^+D^{*-} , respectively. These two channels are related by the isospin symmetry and are relevant for the isoscalar $X(3872)$ with $J^{PC} = 1^{++}$, the isovector $Z_c(3900)$ with $J^{PC} = 1^{+-}$, and the isovector W_{c1} with $J^{PC} = 1^{++}$ pre-

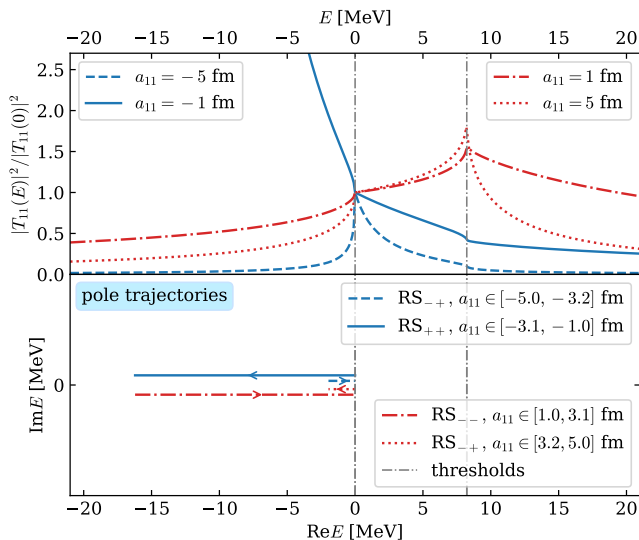


FIG. 2. Line shapes (upper panel) and pole trajectories (lower panel) for the one FP case.

dicted in the hadronic molecular picture in Ref. [37]. For this system, $\delta \equiv \sqrt{2M_2\Delta}$ equals 0.64 fm^{-1} .

As a function on the complex energy (E) plane with branch cuts $[0, +\infty)$ and $[\Delta, +\infty)$ along the positive real- E axis, the two-channel scattering amplitudes have four RSs. The RSs are denoted as $\text{RS}_{r_1 r_2}$ with the subindex representing the signs of $\text{Im } p_1$ and $\text{Im } p_2$; RS_{++} , RS_{-+} , RS_{--} and RS_{+-} correspond to the first to the fourth RS, respectively. The first RS is also called the physical RS, whereas the other three are unphysical ones. The shortest path to each unphysical RS from the physical region (the upper edge of the cut in RS_{++}) is shown in Fig. 1. RS_{-+} and RS_{--} can be reached by crossing the cuts only once and thus are directly connected to the physical region, while RS_{+-} can only be reached by crossing the cuts twice.

Let us first consider the evolution from the single-pole FP. For the two channels related by a symmetry, we have $c = 1/2$ in Eq. (6) as the FP. Evolving a_{11} away from infinity, the pole of Eq. (9) is located at the solution of

$$\frac{2}{a_{11}} - ir_1 p_1 - ir_2 p_2 = 0, \quad (10)$$

on $\text{RS}_{r_1 r_2}$. Equation (10) implies that amplitudes with opposite a_{11} have the same pole positions but on RSs with opposite subindices. This will be called pole duality and the corresponding RSs will be called dual RSs in the following. For $a_{11}\delta < -2$, the effective scattering length $a_{11,\text{eff}} = (2/a_{11} + \delta)^{-1}$ in channel-1 is positive, and one gets a virtual state pole located on RS_{-+} . Increasing a_{11} such that $a_{11,\text{eff}}$ becomes negative, the pole moves to RS_{++} and becomes a bound state pole. Correspondingly, the line shape changes from a narrow threshold cusp to a below-threshold peak, as shown as the blue lines in Fig. 2 (line shapes in the upper panel and pole trajectory in the

lower panel). The trajectory of the pole for positive a_{11} on the dual RS and the corresponding pole line shapes are shown as the red lines in Fig. 2. One sees that there is always a single peak in the line shape. This is the case of Fit 2 in the analysis of the Z_c and Z_{cs} states in Ref. [38], which has more complications due to the existence of triangle singularities [7, 39].

Let us now consider the evolution from the two-pole FP, Eq. (5). The poles of the amplitudes are given by the solutions of

$$\left(\frac{1}{a_{11}} - ir_1 p_1\right) \left(\frac{1}{a_{11}} - ir_2 p_2\right) - \frac{1}{a_{12}^2} = 0, \quad (11)$$

which implies again the pole duality, *i.e.*, the amplitudes with the same $|a_{12}|$ but opposite a_{11} have poles on $\text{RS}_{r_1 r_2}$ and $\text{RS}_{-r_1 -r_2}$, respectively, at the same positions. From

$$\mathbf{T}_{21}(E) = \frac{-2\pi a_{12}^{-1}}{\sqrt{M_1 M_2 \det}}, \quad \mathbf{T}_{11}(E) = \frac{-2\pi (a_{11}^{-1} - ip_2)}{M_1 \det}, \quad (12)$$

with $\det \equiv (a_{11}^{-1} - ip_1)(a_{11}^{-1} - ip_2) - a_{12}^{-2}$, the line shape of \mathbf{T}_{21} is dominated by the poles, while that of \mathbf{T}_{11} is complicated due to a zero at $E = \Delta(1 - a_{11}^{-2}\delta^{-2})$ in addition [13] (see also Ref. [40]).

At the RG FP in Eq. (5), $a_{11} = a_{12} = \infty$ and $\delta = 0$, there are two bound/virtual state poles at $E = 0$, the threshold of both channels. The two poles will separate and be located at $E = 0$ and $E = \Delta$, respectively, for $\delta \neq 0$. For finite a_{11} and a_{12} , using the conformal mapping [35, 41, 42],

$$p_1 = \sqrt{\frac{\mu_1 \Delta}{2}} \left(\omega + \frac{1}{\omega}\right), \quad p_2 = \sqrt{\frac{\mu_2 \Delta}{2}} \left(\omega - \frac{1}{\omega}\right), \quad (13)$$

the four RSs of the complex E plane can be mapped into the ω plane. It is easy to find that there are four poles in the ω plane in total, and thus four poles in all RSs of E plane.

Then we can classify the near-threshold line shapes according to the values of a_{11} and $|a_{12}|$. Cases with a_{11} negative and positive are labeled by B and V, corresponding to having bound and virtual state poles in the single-channel situation, respectively. The line shapes in these two groups of cases are shown in Tables I and II. One sees that the line shapes can be quite different for different values of a_{11} and $|a_{12}|$, however, the evolution can be understood from the pole trajectories, which are shown in the tables as well. The tables may be regarded as a dictionary for the near-threshold line shapes and the corresponding pole locations.

Starting from the near-FP situation $a_{11}\delta \ll -1$ and $1/a_{12} = 0$, each channel has a bound state just below the corresponding threshold. Without channel coupling, each bound state has two poles on different RSs at the same location. That is, the poles of the channel-1 bound state are on RS_{++} and RS_{+-} , while those of the channel-2 bound state are on RS_{++} and RS_{-+} .

TABLE I. Line shapes of T -matrix elements in the near-threshold region for the negative a_{11} cases. Pole trajectories evolving among the cases are shown in the last column. The shadow pole of pole-1 is denoted as Spole-1.

Case	$a_{11}\delta$	$ a_{12} \delta$	Line shapes	Pole trajectories
B1	$\ll -1$	$\gg 1$		
B2	$(-1, 0)$	$\gg 1$		
B3	$(-1, 0)$	$(0, 1)$		
B4	$\ll -1$	$(0, 1)$		

TABLE II. Line shapes of T -matrix elements in the near-threshold region for the positive a_{11} cases. Pole trajectories evolving among the cases are shown in the last column. The shadow pole of pole-1 is denoted as Spole-1.

Case	$a_{11}\delta$	$ a_{12} \delta$	Line shapes	Pole trajectories
V1	$\gg 1$	$\gg 1$		
V2	(0, 1)	$\gg 1$		
V3	(0, 1)	(0, 1)		
V4	$\gg 1$	(0, 1)		

Case B1 ($a_{11}\delta \ll -1$, $|a_{12}|\delta \gg 1$) is obtained by switching on the channel coupling. Both channel-1 poles are pushed downward on their RSs; the one on RS_{++} (pole-1 in Table I) is the main pole since it is close to the physical region while the one on RS_{+-} becomes its shadow (Spole-1) [43] and has little effect on the physical line shape. The channel-2 poles acquire imaginary parts because of the coupling to the lower channel, and become a complex conjugated pair on RS_{-+} (pole-2), as required by the Schwarz reflection principle. In this case, the line shape of $|\mathbf{T}_{21}|$ has two sharp peaks below the two thresholds, while that of $|\mathbf{T}_{11}|$ has a dip just below the higher threshold, as a consequence of the zero of $\mathbf{T}_{11}(E)$ in Eq. (12) [13].

Case B2 ($-1 < a_{11}\delta < 0$, $|a_{12}|\delta \gg 1$) is obtained by increasing a_{11} (corresponding to increasing the single-channel attraction) from Case B1. Both poles move downward. Eventually, the pole-2 conjugated pair move down below the lower threshold on RS_{-+} , then one of them moves upward, transiting to RS_{++} at the lower threshold, and the other moves further downward on RS_{-+} and has little effect on the physical line shape. Correspondingly, two peaks appear in the line shapes.

Case B3 ($-1 < a_{11}\delta < 0$, $|a_{12}|\delta < 1$) is obtained by decreasing $|a_{12}|$ (increasing channel coupling, which introduces an effective attraction in channel-1 and repulsion in channel-2) from Case B2. Pole-1 moves further downward and remotely, while pole-2 moves upward and eventually back to RS_{-+} as a conjugated pair. If pole-2 is above the higher threshold, a sharp threshold cusp at the higher threshold appears (blue solid lines in the line shapes of Case B3 in Table I); if pole-2 is between the two thresholds, a bump appears in the line shapes (red dotted lines).

Case B4 ($a_{11}\delta \ll -1$, $|a_{12}|\delta < 1$) is obtained by increasing $|a_{11}|$ from Case B3. Pole-1 moves upward, and pole-2 moves upward far above the higher threshold. It can happen that pole-1 is close to the lower threshold, or all poles are far from the thresholds; in the latter situation, no prominent near-threshold peak appears in the line shapes. The zero of $\mathbf{T}_{11}(E)$ can still give a dip.

The positive a_{11} cases can be analyzed similarly and are listed in Table II. One distinction compared to the above cases is that the line shapes are threshold cusps except for Case V4 where pole-1 is dragged by the effective attraction due to the strong channel coupling to RS_{++} and gives a peak below the lower threshold. This is the case of the $X(3872)$ discussed in Ref. [37], and pole-2 corresponds to the isovector $J^{PC} = 1^{++} W_{c1}$ predicted therein, which has received support from a recent lattice calculation in Ref. [44].

In all the cases, if the $|\mathbf{T}_{i1}|$ ($i = 1, 2$) line shapes drop monotonically below the lower threshold and above the higher threshold, the width of the peaking structure around the thresholds is controlled by the threshold splitting Δ . We define E_+ and E_- as the energies satisfying

$|\mathbf{T}_{i1}(E_+)| = |\mathbf{T}_{i1}(\Delta)|/2$ and $|\mathbf{T}_{i1}(E_-)| = |\mathbf{T}_{i1}(0)|/2$, respectively, and the half-threshold-heights width as $\Gamma \equiv E_+ - E_-$. Then, we have the following results for Γ of $|\mathbf{T}_{i1}|$:

$$\begin{aligned}\Gamma_{|\mathbf{T}_{21}|(V1)} &= \Delta [1 + \mathcal{O}(a_{11}^{-2}\delta^{-2})], \\ \Gamma_{|\mathbf{T}_{11}|(V2)} &= 4\Delta \left[\frac{1}{(a_{11}\delta)^2} + \frac{1}{a_{11}\delta} + 1 + \mathcal{O}(a_{11}^2\delta^2) \right], \\ \Gamma_{|\mathbf{T}_{21}|(V2)} &= \Delta \left[\frac{7}{4(a_{11}\delta)^2} + \frac{1}{a_{11}\delta} + 3 + \mathcal{O}(a_{11}^2\delta^2) \right], \\ \Gamma_{|\mathbf{T}_{i1}|(B3, V3)} &= \frac{17}{8}\Delta [1 + \mathcal{O}(|a_{11}|\delta)],\end{aligned}\quad (14)$$

where the corresponding cases are given in the parentheses.

IV. SUMMARY

To summarize, the general near-threshold structures in the coupled-channel system have been classified according to the scattering lengths and the channel coupling strength, with the evolution starting from the RG FPs. A symmetry-related two-channel system was discussed as an example, and a dictionary for the evolution of line shapes and the corresponding pole locations was provided in Tables I and II. The results can be used to perceive rough pole locations from line shapes, and thus useful for understanding the complicated line shapes of exotic hadron candidates in the near-threshold region which were observed in recent years and are expected to be observed in the future.

Considering the phase space, the line shapes below the lower threshold considered here can only be observed in the final states of a lower channel. A three-channel discussion is needed for a complete treatment, and the results are similar as reported here if the lowest channel is weakly coupled to the higher two channels [45].

ACKNOWLEDGMENTS

This work is supported in part by the Chinese Academy of Sciences under Grants No. YSBR-101 and No. XDB34030000; by the National Key R&D Program of China under Grant No. 2023YFA1606703; by the National Natural Science Foundation of China (NSFC) under Grants No. 12125507, No. 12361141819 and No. 12047503; and by NSFC and the Deutsche Forschungsgemeinschaft (DFG) through the funds provided to the Sino-German Collaborative Research Center CRC110 ‘‘Symmetries and the Emergence of Structure in QCD’’ (DFG Project-ID 196253076).

- [1] A. Esposito, A. Pilloni, and A. D. Polosa, Multiquark resonances, *Phys. Rept.* **668**, 1 (2017), [arxiv:1611.07920 \[hep-ph\]](#).
- [2] A. Hosaka, T. Iijima, K. Miyabayashi, Y. Sakai, and S. Yasui, Exotic hadrons with heavy flavors: X , Y , Z , and related states, *PTEP* **2016**, 062C01 (2016), [arxiv:1603.09229 \[hep-ph\]](#).
- [3] F.-K. Guo, C. Hanhart, U.-G. Meißner, Q. Wang, Q. Zhao, and B.-S. Zou, Hadronic molecules, *Rev. Mod. Phys.* **90**, 015004 (2018), [arxiv:1705.00141 \[hep-ph\]](#).
- [4] S. L. Olsen, T. Skwarnicki, and D. Zieminska, Nonstandard heavy mesons and baryons: Experimental evidence, *Rev. Mod. Phys.* **90**, 015003 (2018), [arxiv:1708.04012 \[hep-ph\]](#).
- [5] M. Karliner, J. L. Rosner, and T. Skwarnicki, Multi-quark states, *Ann. Rev. Nucl. Part. Sci.* **68**, 17 (2018), [arxiv:1711.10626 \[hep-ph\]](#).
- [6] N. Brambilla, S. Eidelman, C. Hanhart, A. Nefediev, C.-P. Shen, C. E. Thomas, A. Vairo, and C.-Z. Yuan, The XYZ states: Experimental and theoretical status and perspectives, *Phys. Rept.* **873**, 1 (2020), [arxiv:1907.07583 \[hep-ex\]](#).
- [7] F.-K. Guo, X.-H. Liu, and S. Sakai, Threshold cusps and triangle singularities in hadronic reactions, *Prog. Part. Nucl. Phys.* **112**, 103757 (2020), [arxiv:1912.07030 \[hep-ph\]](#).
- [8] H.-X. Chen, W. Chen, X. Liu, Y.-R. Liu, and S.-L. Zhu, An updated review of the new hadron states, *Rept. Prog. Phys.* **86**, 026201 (2022), [arxiv:2204.02649 \[hep-ph\]](#).
- [9] L. Meng, B. Wang, G.-J. Wang, and S.-L. Zhu, Chiral perturbation theory for heavy hadrons and chiral effective field theory for heavy hadronic molecules, *Phys. Rept.* **1019**, 2266 (2023), [arxiv:2204.08716 \[hep-ph\]](#).
- [10] S. K. Choi *et al.* (Belle), Observation of a narrow charmonium-like state in exclusive $B^\pm \rightarrow K^\pm \pi^+ \pi^- J/\psi$ decays, *Phys. Rev. Lett.* **91**, 262001 (2003), [arxiv:hep-ex/0309032](#).
- [11] R. Aaij *et al.* (LHCb), Study of the lineshape of the $\chi_{c1}(3872)$ state, *Phys. Rev. D* **102**, 092005 (2020), [arxiv:2005.13419 \[hep-ex\]](#).
- [12] R. Aaij *et al.* (LHCb), Study of the $\psi_2(3823)$ and $\chi_{c1}(3872)$ states in $B^+ \rightarrow (J/\psi \pi^+ \pi^-) K^+$ decays, *JHEP* **08**, 123, [arxiv:2005.13422 \[hep-ex\]](#).
- [13] X.-K. Dong, F.-K. Guo, and B.-S. Zou, Explaining the Many Threshold Structures in the Heavy-Quark Hadron Spectrum, *Phys. Rev. Lett.* **126**, 152001 (2021), [arxiv:2011.14517 \[hep-ph\]](#).
- [14] S. Navas *et al.* (Particle Data Group), Review of Particle Physics, *Phys. Rev. D* **110**, 030001 (2024).
- [15] R. Aaij *et al.* (LHCb), Observation of structure in the J/ψ -pair mass spectrum, *Sci. Bull.* **65**, 1983 (2020), [arxiv:2006.16957 \[hep-ex\]](#).
- [16] G. Aad, B. K. Abbott, K. Abeling, *et al.* (ATLAS), Observation of an excess of di-charmonium events in the four-muon final state with the ATLAS detector, *Phys. Rev. Lett.* **131**, 151902 (2023), [arxiv:2304.08962 \[hep-ex\]](#).
- [17] A. Hayrapetyan *et al.* (CMS), Observation of new structure in the $J/\psi J/\psi$ mass spectrum in proton-proton collisions at $\sqrt{s} = 13$ TeV, *Phys. Rev. Lett.* **132**, 111901 (2024), [arxiv:2306.07164 \[hep-ex\]](#).
- [18] X.-K. Dong, V. Baru, F.-K. Guo, C. Hanhart, and A. Nefediev, Coupled-Channel Interpretation of the LHCb Double- J/ψ Spectrum and Hints of a New State Near the $J/\psi J/\psi$ Threshold, *Phys. Rev. Lett.* **126**, 132001 (2021), [Erratum: *Phys.Rev.Lett.* 127, 119901 (2021)], [arxiv:2009.07795 \[hep-ph\]](#).
- [19] R. Aaij *et al.* (LHCb), First Observation of a Doubly Charged Tetraquark and Its Neutral Partner, *Phys. Rev. Lett.* **131**, 041902 (2023), [arxiv:2212.02716 \[hep-ex\]](#).
- [20] R. Aaij *et al.* (LHCb), Amplitude analysis of $B^0 \rightarrow \bar{D}^0 D_s^+ \pi^-$ and $B^+ \rightarrow D^- D_s^+ \pi^+$ decays, *Phys. Rev. D* **108**, 012017 (2023), [arxiv:2212.02717 \[hep-ex\]](#).
- [21] R. Molina and E. Oset, $T_{cs}(2900)$ as a threshold effect from the interaction of the $D^* K^*$, $D_s^* \rho$ channels, *Phys. Rev. D* **107**, 056015 (2023), [arxiv:2211.01302 \[hep-ph\]](#).
- [22] R. Aaij *et al.* (LHCb), Observation of an exotic narrow doubly charmed tetraquark, *Nature Phys.* **18**, 751 (2022), [arxiv:2109.01038 \[hep-ex\]](#).
- [23] R. Aaij *et al.* (LHCb), Study of the doubly charmed tetraquark T_{cc}^+ , *Nature Commun.* **13**, 3351 (2022), [arxiv:2109.01056 \[hep-ex\]](#).
- [24] S. Fleming, R. Hodges, and T. Mehen, T_{cc}^+ decays: Differential spectra and two-body final states, *Phys. Rev. D* **104**, 116010 (2021), [arxiv:2109.02188 \[hep-ph\]](#).
- [25] M. Albaladejo, T_{cc}^+ coupled channel analysis and predictions, *Phys. Lett. B* **829**, 137052 (2022), [arxiv:2110.02944 \[hep-ph\]](#).
- [26] M.-L. Du, V. Baru, X.-K. Dong, A. Filin, F.-K. Guo, C. Hanhart, A. Nefediev, J. Nieves, and Q. Wang, Coupled-channel approach to T_{cc}^+ including three-body effects, *Phys. Rev. D* **105**, 014024 (2022), [arxiv:2110.13765 \[hep-ph\]](#).
- [27] R. Aaij *et al.* (LHCb), Observation of a $J/\psi \Lambda$ Resonance Consistent with a Strange Pentaquark Candidate in $B^- \rightarrow J/\psi \Lambda \bar{p}$ Decays, *Phys. Rev. Lett.* **131**, 031901 (2023), [arxiv:2210.10346 \[hep-ex\]](#).
- [28] L. Meng, B. Wang, and S.-L. Zhu, Double thresholds distort the line shapes of the $P_{\psi_s}^\Lambda(4338)^0$ resonance, *Phys. Rev. D* **107**, 014005 (2023), [arxiv:2208.03883 \[hep-ph\]](#).
- [29] R. Aaij *et al.* (LHCb), Observation of a Resonant Structure near the $D_s^+ D_s^-$ Threshold in the $B^+ \rightarrow D_s^+ D_s^- K^+$ Decay, *Phys. Rev. Lett.* **131**, 071901 (2023), [arxiv:2210.15153 \[hep-ex\]](#).
- [30] R. Aaij *et al.* (LHCb), First observation of the $B^+ \rightarrow D_s^+ D_s^- K^+$ decay, *Phys. Rev. D* **108**, 034012 (2023), [arxiv:2211.05034 \[hep-ex\]](#).
- [31] T. Ji, X.-K. Dong, M. Albaladejo, M.-L. Du, F.-K. Guo, and J. Nieves, Establishing the heavy quark spin and light flavor molecular multiplets of the $X(3872)$, $Z_c(3900)$ and $X(3960)$, *Phys. Rev. D* **106**, 094002 (2022), [arxiv:2207.08563 \[hep-ph\]](#).
- [32] V. Lensky and M. C. Birse, Coupled-channel effective field theory and proton- ^7Li scattering, *Eur. Phys. J. A* **47**, 142 (2011), [arxiv:1109.2797 \[nucl-th\]](#).
- [33] D. B. Kaplan, M. J. Savage, and M. B. Wise, A new expansion for nucleon-nucleon interactions, *Phys. Lett. B* **424**, 390 (1998).
- [34] D. B. Kaplan, M. J. Savage, and M. B. Wise, Two nucleon systems from effective field theory, *Nucl. Phys. B* **534**, 329 (1998), [arxiv:nucl-th/9802075](#).
- [35] F.-K. Guo, C. Hanhart, Yu. S. Kalashnikova, P. Matuschek, R. V. Mizuk, A. V. Nefediev, Q. Wang, and J. L.

- Wynen, Interplay of quark and meson degrees of freedom in near-threshold states: A practical parametrization for line shapes, *Phys. Rev. D* **93**, 074031 (2016), [arXiv:1602.00940 \[hep-ph\]](#).
- [36] T. D. Cohen, B. A. Gelman, and U. van Kolck, An effective field theory for coupled channel scattering, *Phys. Lett. B* **588**, 57 (2004), [arXiv:nucl-th/0402054](#).
- [37] Z.-H. Zhang, T. Ji, X.-K. Dong, F.-K. Guo, C. Hanhart, U.-G. Meißner, and A. Rusetsky, Predicting isovector charmonium-like states from X(3872) properties, (2024), [arXiv:2404.11215 \[hep-ph\]](#).
- [38] V. Baru, E. Epelbaum, A. A. Filin, C. Hanhart, and A. V. Nefediev, Is $Z_{cs}(3982)$ a molecular partner of $Z_c(3900)$ and $Z_c(4020)$ states?, *Phys. Rev. D* **105**, 034014 (2022), [arXiv:2110.00398 \[hep-ph\]](#).
- [39] Q. Wang, C. Hanhart, and Q. Zhao, Decoding the riddle of Y(4260) and $Z_c(3900)$, *Phys. Rev. Lett.* **111**, 132003 (2013), [arXiv:1303.6355 \[hep-ph\]](#).
- [40] K. Sone and T. Hyodo, General amplitude of near-threshold hadron scattering for exotic hadrons, (2024), [arXiv:2405.08436 \[hep-ph\]](#).
- [41] M. Kato, Analytical properties of two-channel S-matrix, *Annals Phys.* **31**, 130 (1965).
- [42] W. A. Yamada, O. Morimatsu, T. Sato, and K. Yazaki, Near-threshold spectrum from a uniformized Mittag-Leffler expansion: Pole structure of the $Z(3900)$, *Phys. Rev. D* **105**, 014034 (2022), [arXiv:2108.11605 \[hep-ph\]](#).
- [43] R. J. Eden and J. R. Taylor, Poles and Shadow Poles in the Many-Channel S Matrix, *Phys. Rev.* **133**, B1575 (1964).
- [44] M. Sadl, S. Collins, Z.-H. Guo, M. Padmanath, S. Prelovsek, and L.-W. Yan, Charmoniumlike channels 1^+ with isospin 1 from lattice and effective field theory, (2024), [arXiv:2406.09842 \[hep-lat\]](#).
- [45] Z.-H. Zhang, X.-Y. Zhang, and F.-K. Guo, (2024), in preparation.